Elastic and inelastic low-energy electron collisions with pyrazine

Journal Item

Elastic and inelastic low-energy electron collisions with pyrazine

Zdeněk Mašín[a] and Jimena D. Gorfinkiel[b]
Department of Physics and Astronomy, The Open University, Walton Hall, Milton Keynes, MK7 6AA, United Kingdom

(Received 3 June 2011; accepted 21 September 2011; published online 14 October 2011)

We present results of *ab-initio* scattering calculations for electron collisions with pyrazine using the R-matrix method, carried out at various levels of approximation. We confirm the existing experimental and theoretical understanding of the three well-known π^* shape resonances. In addition, we find numerous core-excited resonances (above 4.8 eV) and identify their most likely parent states. We also present differential cross sections, showing high sensitivity to the scattering model chosen at low energies. We make recommendations regarding the selection of models for scattering calculations with this type of targets. © *2011 American Institute of Physics*. [doi:10.1063/1.3650236]

I. INTRODUCTION

Studies of low-energy electron collisions with biomolecules are motivated by their importance in the understanding of radiation damage, particularly to DNA.[1] Additionally, high-level theoretical studies of inelastic electron collisions with large molecules are still scarce, and therefore interesting in their own right.

It is well known that the electron resonances present in DNA bases provide a doorway for low-energy electron induced damage to DNA and RNA.[2–4] Three π^* electron resonances have been found experimentally in the four DNA bases and in uracil.[5,6] It has been proposed[6–11] on the basis of experimental evidence, that the lowest-energy features (below 3 eV) in the dissociative electron attachment (DEA) spectra of the bases do not correspond directly to any of these π^* resonances but are rather caused by the formation of vibrational Feshbach resonances[11,12] and by an interaction, mediated by nuclear motion, between the π^* resonances and a possible σ^* resonance occurring in this energy region.

Apart from the well-studied lower energy region, the total DEA cross section for the pyrimidinic DNA bases also shows a significant enhancement in the higher-energy range (from 5 eV to 9 eV),[13–15] comparable in magnitude to the one observed at the lower energies, which is thought to be caused in this case by core-excited resonances.[15,16] Recent measurements[17] of the electronic excitation cross sections of cytosine by low energy electrons have also provided evidence for the presence of higher-lying core-excited resonances in this system.

Uracil is the base molecule with the smallest number of electrons, and therefore the most studied target in scattering calculations from pyrimidinic bases. Theoretical calculations of electron collisions with uracil by Gianturco *et al.*[18,19] and Winstead and McKoy[20] suggest the presence of at least one higher-lying broad σ^* shape resonance located at energies above 8 eV, much higher-than the σ^* resonance postulated by others.[11] Consequently it has been proposed[19] that the observed products[13] of the electron-uracil collision can also be explained by an interaction between the higher-lying (above 8 eV) dissociative σ^* resonance and the lower-lying π^* resonances.

To the best of our knowledge the only *inelastic* and fully *ab initio* calculations of electron collisions with pyrimidine-like molecules are those of Winstead and McKoy[20] using the Schwinger multichannel method (SMC) and Dora *et al.*[21] using the R-matrix method, on electron collisions with uracil. The calculations of Winstead and McKoy found evidence for Feshbach resonances in the electron-uracil system, but did not characterize them, while the subsequent study of Dora *et al.* found three Feshbach resonances at energies 6.17 eV, 7.62 eV, and 8.12 eV.

In addition to the poor characterization of the possible higher-lying resonances in pyrimidine DNA bases, previous studies[18–20,22–25] have struggled to produce parameters of, especially, the third (highest-lying) π^* resonance in satisfactory agreement with experimental values. For this reason, Winstead and McKoy investigated elastic electron collisions with a model molecule, pyrazine.[26,27] Pyrazine ($C_4H_4N_2$), an isomer of pyrimidine, is a good model for the pyrimidinic nucleobases and is particularly useful for theoretical calculations because of its high symmetry, D_{2h}, which has the further advantage of making the molecule non-polar.

Electron collisions with pyrazine were studied experimentally by Nenner and Schulz[28] in 1975. They identified three low-lying π^* shape resonances below 5 eV in this system. The two lowest-lying resonances (at 0.065 and 0.87 eV) were suggested to have a pure shape character while the third one, found at about 4.10 eV, was suggested to have a mixed shape and core-excited character arising from mixing of the resonance with the lowest-lying triplet excited electronic states of pyrazine. The calculations of electron collisions with pyrazine by Winstead and McKoy[26,27] have indeed provided strong evidence for the mixed shape and core-excited character of this resonance.

Our theoretical work uses the R-matrix method for the study of elastic and inelastic collisions of electrons with pyrazine. We investigate the whole energy region below the ionization threshold of the molecule, with particular care

[a]Electronic mail: z.masin@open.ac.uk.
[b]Electronic mail: j.gorfinkiel@open.ac.uk.

devoted to the higher energy range, in order to look for the presence of core-excited shape or Feshbach resonances not reported for this molecule before. As a starting point for the construction of our scattering models, we choose those devised by Dora *et al*. in their study[21] of electron collisions with uracil.

The electronic excited states of pyrazine, important for the inelastic part of our calculations, have been studied extensively by experimental[29–31] and theoretical quantum chemistry methods.[32–36] The latter provide a basis for the description of the electronic excited states in our scattering calculations. These studies have reported that most of these states are valence in character with the exception of perhaps just four higher-lying (found in calculations above 7 eV) Rydberg singlet states[32] and a diffuse $^3B_{2u}$ (Ref. 34) state with an experimentally determined vertical excitation energy of about 4.50 eV.[29] It is worth mentioning that pyrazine is a molecule with positive electron affinity, i.e., it supports a bound state of the singly charged negative ion of $^2B_{3u}$ symmetry. Its experimentally determined vertical ionization energy is 9.63 eV.[37]

II. THEORY

Our scattering calculations were performed using the R-matrix method as implemented in the UK molecular R-matrix codes.[38] The R-matrix theory has been described in detail elsewhere,[39,40] and therefore we give just a brief description here.

In the R-matrix method, the configuration space of the electron-molecule collision problem is divided into two parts, the inner region and the outer region. The solution of the scattering problem proceeds by solving first the more complex inner region problem. This is done by diagonalizing the full Hamiltonian of the scattering electron-molecule system inside a sphere with a radius $r = a$ large enough to enclose the whole charge density of the N electrons in the target states of interest (and the L^2 functions).

The Hamiltonian is diagonalized in the basis of $(N + 1)$ electron configurations $\Phi_i \frac{u_{ij}(r)}{r}$ and χ_i. The eigenvectors are written in the close-coupling (CC) form as follows:

$$\Psi_k^\Gamma(\mathbf{X_{N+1}}) = \mathcal{A} \sum_{i=1}^{n} \sum_{j=1}^{n_c} \Phi_i(\mathbf{X_N}; \hat{\mathbf{r}}_{\mathbf{N+1}}; \sigma_{\mathbf{N+1}}) \times \frac{u_{ij}(r_{N+1})}{r_{N+1}} a_{ijk} + \sum_{i=1}^{m} \chi_i(\mathbf{X_{N+1}}) b_{ik}, \quad (1)$$

where each of the functions $\Phi_i(\mathbf{X_N}; \hat{\mathbf{r}}_{\mathbf{N+1}}; \sigma_{\mathbf{N+1}})$ is built from the wavefunctions $\Phi_i(\mathbf{X_N})$ of one of the n target states included in the calculation multiplied by the angular (spherical harmonics $Y_{lm}(\hat{\mathbf{r}}_{\mathbf{N+1}})$) and spin functions, $\sigma_{\mathbf{N+1}}$, of the scattering electron in such a way as to satisfy the spin-space symmetry Γ of $\Psi_k^\Gamma(\mathbf{X_{N+1}})$. The $u_{ij}(r_{N+1})$ are linear combinations of Gaussian functions, which describe the radial behaviour of the scattering electron. Finally the L^2-integrable functions $\chi_i(\mathbf{X_{N+1}})$, crucial for representation of resonances, introduce the correlation between the scattering electron and those in the molecule. The operator $\mathcal{A}$ guarantees the correct antisymmetrization of the whole wavefunction.

The coefficients a_{ijk} and b_{ik} are then determined from the requirement

$$\left\langle \Psi_{k'}^\Gamma \middle| H_{N+1} + L \middle| \Psi_k^\Gamma \right\rangle = E_k \delta_{k'k}, \quad (2)$$

where L is the Bloch operator, whose precise form is given, e.g., in Tennyson (2010),[39] H_{N+1} is the fixed-nuclei Hamiltonian of the electron-molecule system and the eigenvalues E_k are called the R-matrix poles.

In the outer region $r \geq a$, exchange between the scattering electron and electrons of the target is neglected and a single centre expansion of the electron-molecule interaction is used. The R-matrix is constructed and propagated to a radius large enough so that an asymptotic expansion for the radial wavefunctions of the scattering electron in each channel can be used.

The simplest scattering model we employ is the static exchange (SE) model in which only one target wavefunction (for the ground state of the molecule), represented at the Hartree-Fock level, is included in expansion (1). The L^2 functions $\chi_i(\mathbf{X_{N+1}})$ also take a simple form, which reflects the nature of the SE approximation that the target molecule is not allowed to relax (polarize) in the presence of the incoming electron. We can write these configurations in the following way:

$$\chi_i^{SE} : (\text{ground state})^N (\text{virtual})^1, \quad (3)$$

which represent the N electrons of the target molecule occupying the ground state (HF) configuration, while the scattering electron enters one of a selected number of virtual orbitals. The SE approximation is capable of describing only shape electron resonances, but these appear too high in energy due to an incomplete modeling of the correlation between the target and the scattering electron.

At the level of the static exchange plus polarization (SEP) approximation, we still include only the ground state wavefunction in expansion (1), but the molecule is now allowed to be polarized by the incoming electron, which is reflected in the choice of the L^2 configurations. In addition to those described by (3), we include configurations of the type,

$$\chi_i^{SEP} : (\text{core})^{N_c} (\text{valence})^{N-N_c-1} (\text{virtual})^{1+1}, \quad (4)$$

where the core orbitals of the molecule are always doubly occupied by N_c electrons and the molecule is allowed to polarize by promoting one electron from the valence space to the selected number of virtual orbitals, which are also available for the scattering electron. The SEP approximation as described can also reveal core-excited resonances associated with single excitations of the target molecule.

The most sophisticated model we use is the close-coupling approximation in which the eigenfunctions $\Psi_k^\Gamma(\mathbf{X_{N+1}})$ have the full form (1) with a number of target electronic excited states included. One of the most important aspects of scattering calculations based on the CC expansion is that of balance. This means that the description of the N electron target electronic states $\Phi_i(\mathbf{X_N})$ should be of the same quality as description of the $N + 1$ electron basis functions $\Psi_k^\Gamma(\mathbf{X_{N+1}})$ of the electron-molecule collision problem. This requirement is reflected in a particular choice of the target configuration interaction (CI) model and the L^2 functions to be included in (1). In our calculations, we choose to base

our target models around the complete active space (CAS) CI representation of the target wavefunction. This model has been found to produce a satisfactorily balanced results for small targets[41] when a simple set of L^2 functions suffices. Here, we need to expand this model in order to achieve a good description of the resonances and balance is therefore harder to achieve. The precise choice of the number and type of the orbitals as well as a detailed description of the configurations chosen for the three scattering models just introduced will be expounded on later.

III. TARGET MODELS

We used the geometry of pyrazine as determined from experiment[30] and chose to lie the molecule in the *yz* plane, with the nitrogen atoms located along the *z* axis. Pyrazine has 42 electrons and the ground state configuration (for simplicity, the orbitals are not listed in energy order) $a_g^{12} b_{3u}^2 b_{2u}^8 b_{1g}^2 b_{1u}^{10} b_{2g}^2 b_{3g}^6$.

In order to obtain optimal target orbitals for the description of the scattering process, several basis sets were tested. We have found our scattering results particularly sensitive to the quality of the target orbital description, and we therefore extended the analysis of basis set choice carried out by Dora *et al.*[21] Specifically Dora *et al.* used the basis set cc-pVDZ for their calculations on uracil, while for their calculations on pyrazine Winstead and McKoy[26] used a larger 6-311++G** basis set, containing diffuse functions on all atoms; we tested these and another three similar basis sets. We used the Hartree-Fock SCF and the state-averaged CASSCF (SA-CASSCF) methods to generate the target orbitals; the calculations were performed using MOLPRO 2009.1.[43] The use of the modified virtual orbitals (MVO) (Ref. 42) in SE scattering models of our type had already been tested[21] and no significant differences found in the scattering results when compared with calculations using the HF orbitals.

Since the number of configurations included in our scattering calculations based around the CAS model scales rapidly with the size of the active space, we chose to use the smallest realistic active space (10, 8) (Ref. 34) for our SA-CASSCF calculations. This active space comprises 10 electrons distributed among the 6 valence π orbitals and the two lone-pair σ orbitals located on the two nitrogen atoms. Consequently the frozen core in pyrazine comprises the orbitals: 1-5a_g, 1-4b_{2u}, 1-4b_{1u} and 1-3b_{3g}. In the case of uracil, Dora *et al.* used the full π valence space augmented only by the lone-pair orbitals located on the two oxygen atoms.

We tested several averaging schemes in the SA-CASSCF calculations, but found only small differences between the calculated vertical excitation energies of the electronic states. Our preferred scheme includes the two lowest-lying excited states of each spatial and spin symmetry (singlet and triplet) and the ground state, i.e., 32 + 1 states. Table I demonstrates clearly the insensitivity of the calculated excitation energies to the averaging scheme chosen: comparison with the results of Weber and Reimers,[34] who used the same active space and the *state-specific* mode of the CASSCF calculations, in which each of the calculated excited states (and their target orbitals) were optimized individually shows small differences. In our CC scattering calculations, we used the orbitals obtained with the SA-CASSCF method to generate all electronic excited states with excitation energies lying below ≈10 eV. The

TABLE I. Vertical excitation energies, in eV, for the electronic excited states of pyrazine used in our averaging scheme (the two upper panels) and additional third electronic excited states lying below 10 eV (bottom panel). For the singlet states, their character (valence or Rydberg) as determined in the work of Woywod *et al.* (Ref. 32) is given as a subscript to the number of each state. The first two lines in each of these panels present results of our SA-CASSCF calculations using the active space (10, 8) and basis sets cc-pVDZ and 6-311+G** respectively. The CASSCF calculations of Weber and Reimers used the state-specific optimization, cc-pVDZ basis set and the active space (10, 8). Woywod *et al.* used aug cc-pVTZ basis functions on heavy atoms, cc-pVTZ basis functions on hydrogen atoms and the active space (10, 8) for the valence excited states. For the Rydberg states, an augmented active space (10, 9) was used.

	^1A_g		$^1B_{3u}$		$^1B_{2u}$		$^1B_{1g}$		$^1B_{1u}$		$^1B_{2g}$		$^1B_{3g}$		^1A_u	
Excited state	2_V	3_V	1_V	2_R	1_V	2_V	1_V	2_R	1_V	2_V	1_V	2_V	1_V	2_V	1_V	2_R
cc-pVDZ	8.34	8.46	4.84	10.04	4.95	10.03	7.27	10.55	8.67	10.60	5.91	9.03	8.35	11.70	5.98	11.33
6-311+G**	8.25	8.36	4.80	9.96	4.88	9.94	7.24	10.42	8.59	10.46	5.84	8.99	8.28	11.69	6.00	11.17
Observed[a]	…	…	3.97	…	4.81	7.67	6.10	7.13[b]	6.51	7.67	5.19	…	…	…	4.72[c]	…
Weber and Reimers	…	…	4.86	…	5.05	10.03	7.20	…	8.56	10.53	5.91	…	…	…	5.92	…
Woywod *et al.*	8.39	11.66	4.87	7.28	4.96	9.83	7.23	7.37	8.35	10.21	5.87	9.12	8.30	11.19	6.01	7.45

	^3A_g		$^3B_{3u}$		$^3B_{2u}$		$^3B_{1g}$		$^3B_{1u}$		$^3B_{2g}$		$^3B_{3g}$		^3A_u	
Excited state	1	2	1	2	1	2	1	2	1	2	1	2	1	2	1	2
cc-pVDZ	7.34	12.51	4.18	9.84	4.89	8.20	7.13	10.41	3.90	5.15	5.34	8.82	7.46	10.10	5.93	11.06
6-311+G**	7.27	12.38	4.16	9.77	4.81	8.15	7.09	10.29	3.86	5.10	5.28	8.77	7.40	10.08	5.95	10.92
Observed[a]	…	…	3.42	…	4.5	…	…	…	4.0	5.7	4.59	…	…	…	4.2	…
Weber and Reimers	…	…	4.23	…	4.81	…	…	…	4.00	5.32	5.33	…	…	…	5.86	…

Excited state	$3\,^3B_{3u}$	$3\,^3B_{2g}$	$3\,^3B_{1u}$
cc-pVDZ	10.01	9.05	8.65
6-311+G**	9.92	9.00	8.56

[a]Weber and Reimers (Ref. 34) if a different reference is not given.
[b]Oku *et al.* (Ref. 31).
[c]Li *et al.*. (Ref. 33).

TABLE II. Ground state energies of pyrazine (in hartree) calculated using the Hartree-Fock and SA-CASSCF methods and energies (in eV) of the orbitals used in the active space together with the first SA-CASSCF virtual orbitals of each irreducible representation. The virtual orbitals are ordered according to their energies as calculated using the 6-311+G** basis set. Details of the SA-CASSCF calculations are given in the text.

	Basis set	cc-pVDZ	aug cc-pVDZ	cc-pVTZ	6-311+G**	6-311++G**
	Hartree-Fock energy	− 262.69726	− 262.70930	− 262.76069	− 262.73551	− 262.73558
	SA-CASSCF(10,8) energy	− 262.77481	− 262.78472	− 262.83669	− 262.81221	− 262.81227
	Number of GTOs	104	174	236	156	160
Active space orbs.	$1b_{3u}$ (π)	− 14.814	− 14.950	− 14.895	− 14.970	− 14.969
	$5b_{1u}$ (σ)	− 11.897	− 12.033	− 11.952	− 12.058	− 12.057
	$1b_{2g}$ (π)	− 11.347	− 11.506	− 11.446	− 11.540	− 11.539
	$6a_{g}$ (σ)	− 9.515	− 9.675	− 9.619	− 9.719	− 9.718
	$1b_{1g}$ (π)	− 8.406	− 8.484	− 8.438	− 8.538	− 8.537
	$2b_{3u}$ (π)	− 0.542	− 0.794	− 0.700	− 0.848	− 0.847
	$1a_{u}$ (π)	1.955	1.770	1.860	1.734	1.735
	$2b_{2g}$ (π)	8.260	8.123	8.191	8.046	8.047
Virtual orbs.	$7a_{g}$ (σ)	5.380	0.967	4.256	1.770	1.163
	$5b_{2u}$ (σ)	5.804	1.145	4.547	2.101	1.291
	$6b_{1u}$ (σ)	6.469	1.290	5.204	2.210	1.596
	$4b_{3g}$ (σ)	6.640	1.573	5.295	2.686	1.798
	$3b_{3u}$ (π)	17.943	2.843	11.414	3.075	3.076
	$3b_{2g}$ (π)	20.023	3.283	13.142	3.680	3.681
	$2b_{1g}$ (π)	19.337	3.706	12.580	3.956	3.956
	$2a_{u}$ (π)	21.605	4.701	14.898	5.190	5.190

excitation thresholds for the additional states (those not included in the averaging procedure) are shown at the bottom of Table I. Our calculated values for the vertical excitation energies differ only marginally (±0.16 eV) between the basis sets cc-pVDZ and 6-311+G**.

Table II summarizes the results for the SA-CASSCF pyrazine orbitals and all tested basis sets. We can see that although the energy of the orbitals in the active space does not differ significantly, that of the virtual orbitals, i.e., the orbitals not included in the frozen core or in the active space, differs very much when calculated using compact basis sets, i.e., those not containing diffuse functions. Figure 1 shows the radial charge densities of orbitals $4b_{3g}$ and $3b_{2g}$, and illustrates the significant differences in the shape of the virtual orbitals when calculated in the basis sets cc-pVDZ and 6-311+G**. Similar differences are observed for all the other virtual orbitals calculated in these two basis sets. Conversely the orbitals of the active space do not differ much as is exemplified by the radial charge density of the orbital $5b_{1u}$. As we will see from the results of our scattering calculations, the virtual orbitals play a key role in modeling correlation between the molecular and the scattering electrons: cross sections, especially at lower energies, are significantly different depending on whether compact or diffuse basis sets are used. On this basis, we suggest that the selection of an optimal basis set for scattering calculations on large molecules, when using the models presented below, should not be based solely on the comparison of "integral" values (e.g., the ground state energies and dipole moment if the molecule possesses one) but also on an assessment of the quality of the virtual orbitals. The basis sets for scattering calculations should describe the occupied and virtual orbitals to a similar level of quality.

Taking these considerations into account we should choose (when using SA-CASSCF orbitals) as the optimal basis set one of the diffuse ones (aug cc-pVDZ, 6-311+G** or 6-311++G**), which give significantly lower energies for the virtual orbitals. The last two not correlation-consistent diffuse

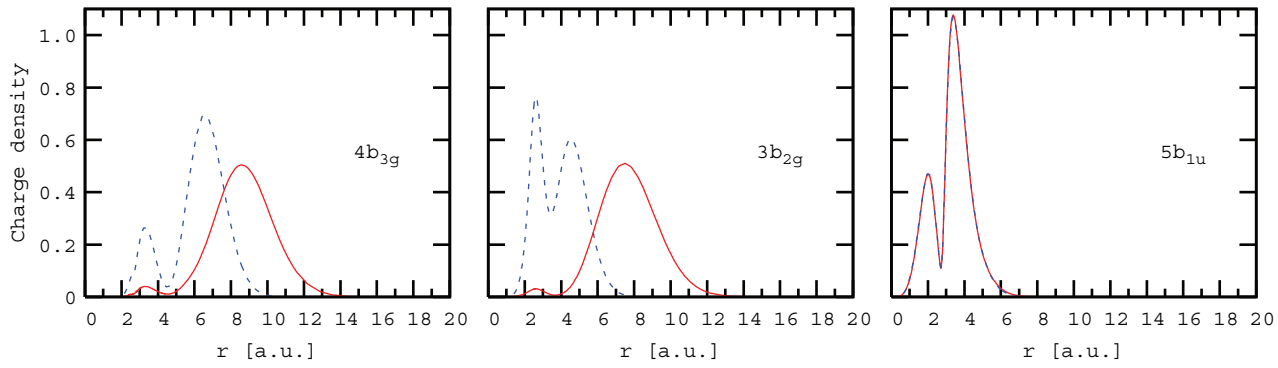

FIG. 1. Radial charge densities of SA-CASSCF orbitals $4b_{3g}$, $3b_{2g}$ and $5b_{1u}$ as calculated in the basis sets cc-pVDZ (dashed blue) and 6-311+G** (solid red). The densities were calculated using a new module, which is scheduled to be incorporated in the forthcoming release of the UK R-matrix codes (Ref. 38).

basis sets give lower values of the ground state energies compared with the aug cc-pVDZ. Use of the 6-311++G** basis set would require larger R-matrix radii than is currently possible (see later). Therefore, we choose as optimal the 6-311+G** basis set, which presents an excellent compromise between size, diffuseness and the quality of the target description.

Nonetheless, we have also used the cc-pVDZ basis set in our scattering calculations in order to ascertain the effect on the collisional data of using a compact basis set and for a qualitative comparison with the results obtained by Dora *et al.* for uracil.

IV. SCATTERING CALCULATIONS

In the scattering calculations, we used both the Hartree-Fock and the CASSCF orbitals obtained by the averaging procedure described above. The continuum Gaussian-type orbitals (GTOs) centred on the centre of mass of the molecule are Schmidt orthogonalized to these (orthogonal) orbitals. The retained continuum orbitals are then symmetric-orthogonalized among themselves. In order to avoid linear dependence problems, only those continuum orbitals of each symmetry, whose eigenvalue is higher than some specified threshold, are retained in the calculation. (The precise selection of those deletion thresholds is described later.)

The main parameters that affect the scattering part of our calculations are the R-matrix radius a and the choice of the continuum GTOs. The latter have to be optimized for each specific radius. The GTOs we used contained functions up to g-wave ($l \leq 4$). In order to check that the assumption of zero amplitude of target electrons density on the R-matrix sphere is satisfied, we performed tests with R-matrix radii (and the corresponding basis sets) of $13a_0$, $15a_0$ and $18a_0$. (The basis set for radius $a = 13a_0$ was optimized by Faure *et al.*,[44] the one for $a = 15a_0$ was optimized by Bouchiha *et al.*[45] and the basis set for radius $a = 18a_0$ is due to Tarana.[46])

We can now turn to the description of our scattering models and results. From now on we will refer to the basis set 6-311+G** as "diffuse" and the cc-pVDZ basis set as "compact." Our scattering calculations do not exhibit convergence of the positions of resonant structures with respect to the number of virtual orbitals included; we observe a behaviour for the positions of the three ^2A_u, $^2B_{2g}$ and $^2B_{3u}$ π^* resonances quantitatively very similar to the one observed by Dora[21] on uracil. Therefore, the optimal number of virtual orbitals used was chosen to give, within a specific model (SEP or close-coupling), positions of the three π^* resonances as close to the experimental ones as possible without overcorrelating any of them. Consequently a scattering calculation will be called overcorrelated if one of these resonances appears in our calculations at lower energy than its experimentally determined position.

A. SE and SEP calculations

On these levels of approximation only the elastic channel is open; the response of the target to the incoming electron is taken into account only in the SEP approximation as described in Sec. II. For both types of calculations, the SA-CASSCF orbitals performed marginally worse than the HF orbitals, and therefore for the SE and SEP calculations, we present results for the HF orbitals only.

The quality of description of the radial wavefunction of the scattering electron in the inner region is strongly related to the deletion thresholds used in the orthogonalization step for the continuum orbitals. For the calculations using R-matrix radii up to $a = 15a_0$, the deletion thresholds were for all symmetries set to the value 1×10^{-7}.

For the calculations using the diffuse basis set and the largest R-matrix radius $a = 18a_0$, the deletion thresholds had to be decreased, as expected,[50] in some symmetries to prevent removing too many continuum functions and give a satisfactory description of the continuum. The optimization of the deletion thresholds was done at the level of the SEP calculations, which will be described below. The deletion thresholds so obtained are listed in Table III.

We included the 25 lowest-lying virtual orbitals in the calculations using both target basis sets. Figure 2 shows the resulting eigenphase sums for all symmetries. For the compact basis set, the results show clearly the presence of the three π^* resonances and some structure in the eigenphase sums above 10 eV. An R-matrix radius as small as $a = 13a_0$ gives SE results nearly identical to the ones obtained using radius $a = 15a_0$ (not shown). Also, no linear dependence problems were observed in any of the calculations using this basis set.

The eigenphase sums have more structure in the case of the calculations using the diffuse basis set. Calculations were initially performed with $a = 15a_0$, but this proved to be too small to contain all the target orbitals' density. In particular, the structure around 3 eV in the B_{3g} symmetry is unphysical, because it disappears completely when $a = 18a_0$ is used. The unphysical origin of this "step" was also confirmed by our calculations of the radial charge densities of the target orbitals, which indeed showed that the B_{3g} symmetry contains the most diffuse orbitals with some of these having an amplitude $\approx 10^{-3}$ for $r = 15a_0$. For this reason $a = 18a_0$, a value for which the amplitudes of all molecular orbitals is $\ll 10^{-3}$, was used in all later calculations with the diffuse basis set.

In order to further assess the stability of the eigenphase sums calculated using the diffuse basis set and $a = 18a_0$, we performed SE calculations using a different continuum basis set, obtained by rescaling the original one by multiplying all the exponents by the factor $\left(\frac{18}{16}\right)^2$; this allowed us to use a slightly higher number of continuum functions in some symmetries, while keeping the deletion thresholds the same as shown in Table III. Any residual linear dependence present in our calculations will lead to the appearance of non-physical R-matrix poles, which in turn may lead to spurious structures

TABLE III. Deletion thresholds for the continuum functions used in the calculations with the 6-311+G** basis set and $a = 18a_0$.

A_g	B_{3u}	B_{2u}	B_{1g}	B_{1u}	B_{2g}	B_{3g}	A_u
10^{-9}	10^{-7}	10^{-7}	10^{-9}	10^{-7}	10^{-7}	6.10^{-7}	10^{-10}

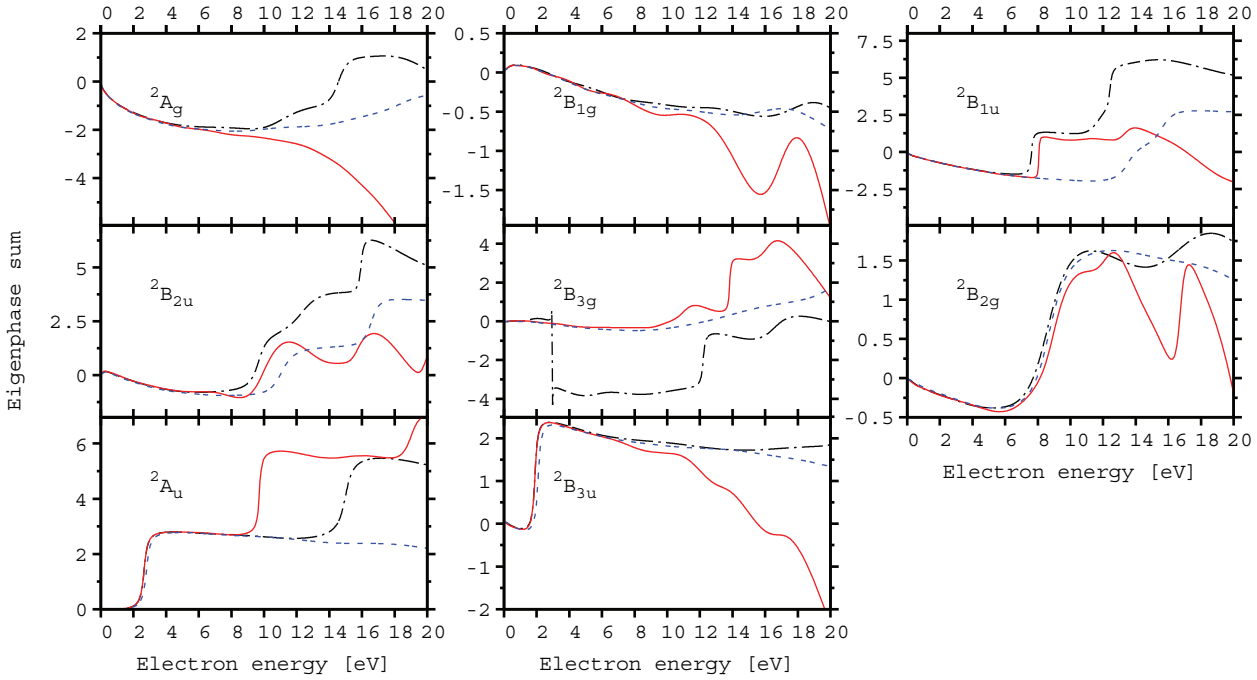

FIG. 2. Eigenphase sums for scattering in all symmetries of pyrazine at the static exchange level. Solid red: calculations performed using the basis set 6-311+G** and R-matrix radius $a = 18a_0$. Dash-dotted black: basis set 6-311+G** and $a = 15a_0$. Short dashed blue: basis set cc-pVDZ and $a = 13a_0$.

in eigenphase sums and cross sections. Changes in the continuum description are reflected in a change of the values of the R-matrix poles. We then expect any unphysical structures to change their position or appearance significantly, while physical structures should remain the same provided that the quality of the description of the continuum is sufficient. We can see in Figure 2 that the second "step" in the A_u symmetry changes its position considerably when the R-matrix radius (and the continuum basis set) are changed from $a = 18a_0$ to $a = 15a_0$, suggesting that this feature might be unphysical. In the SE calculations using the rescaled continuum basis set and the radius $a = 18a_0$, this structure moves to very high energies (around 17 eV) proving again its instability: hence we regard it as unphysical. All other structures remain virtually unchanged.

We will make assignments of the structures present in Figure 2 in terms of resonances later. Here we just note that use of the diffuse basis set, which gives target orbitals of a better quality, results in the shift of some of the structures in the eigenphase sums, e.g., in the B_{1u} symmetry, to considerably lower energies when compared with the calculations using the compact basis set, stressing the importance of choosing a basis set that represents the virtual orbitals sufficiently well. We also note that some of the apparent structure in the higher energy range for the calculation with $a = 18a_0$ are likely to be due to a poor representation of the continuum.

1. SEP calculations

For the SEP calculations, we used the L^2 functions (3) and (4) with the number of virtual orbitals included dependent on the basis set employed. We always include all singlet and triplet-coupled single excitations from the valence space of 15 orbitals of pyrazine to the selected space of the virtual orbitals. For the compact basis set, use of the 25 lowest-lying virtual orbitals was found to give the best results, while for the diffuse basis set using 40 lowest-lying virtual orbitals were found to be optimal. Cross sections for SEP calculations are shown in Figure 3: the rich structure visible in the energy range above 5 eV is inherent to the approximation of this type and corresponds to (non-physical) pseudoresonances. Table IV presents our calculated positions and widths for the three π^* resonances together with the results of the SEP calculations of Winstead and McKoy, who however do not determine the widths of any of these resonances.

We can see from the Table IV that the calculation using the diffuse basis set gives results in better agreement with experiment. This calculation also reveals the Ramsauer-Townsend minimum in the A_g symmetry lying below 0.5 eV as reported earlier by Winstead and McKoy. The largest discrepancy with experimental results occurs for the core-excited shape resonance in B_{2g} symmetry. This discrepancy is not caused by the lack of L^2 functions built on the triplet excited configurations, which Winstead and McKoy found essential for obtaining a good position of this resonance, but we ascribe it to the treatment of polarization in our calculations. Increasing the number of virtual orbitals used in the scattering calculations lowers the positions of all resonances. If we increase the number of virtual orbitals to 35 in the calculation using the compact basis set, the $^2B_{3u}$ resonance becomes bound, while the ^2A_u and $^2B_{2g}$ resonances drop by about 0.25 and 0.5 eV in energy respectively. A similar effect is noticed when the number of virtual orbitals is increased in the calculations with the diffuse basis set (see Table IV). However, the Ramsauer-Townsend minimum remains absent from the calculation with the compact basis set and the ^2A_u resonance drops below the

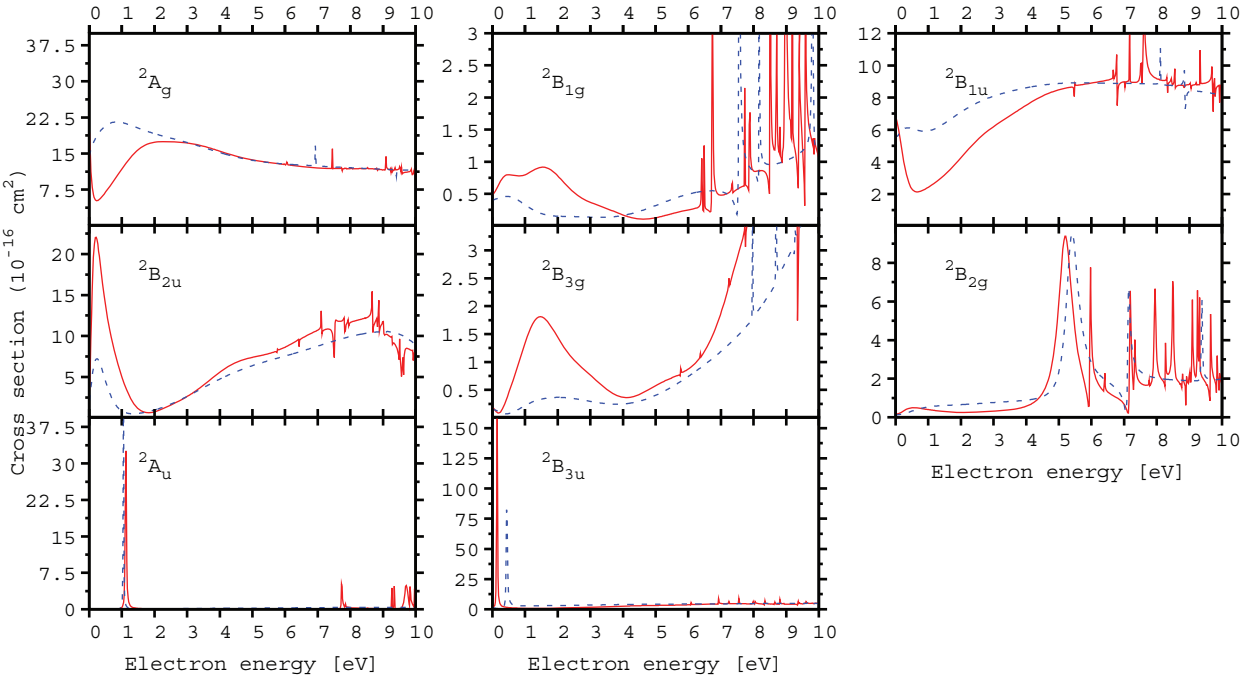

FIG. 3. Contributions to the cross section from all scattering symmetries at the static exchange plus polarization level. Solid red: calculations performed using the basis set 6-311+G** and R-matrix radius $a = 18a_0$. Short dashed blue: basis set cc-pVDZ and $a = 13a_0$.

range indicated by Nenner and Schulz. The calculation using the diffuse basis set continues to provide better agreement with experiment.

The reason for the need to include a higher number of virtual orbitals in the SEP calculation using the 6-311+G** basis set lies in their diffuse character: it would seem that the lower HF virtual orbitals do not describe as much correlation as the ones calculated in the compact basis set. As the energy of the scattering electron increases, modeling of the correlation between it and the molecule becomes more difficult. We can also see from our calculations of the vertical excitation energies of the electronic excited states of pyrazine (see Table I), that the discrepancy between the measured and calculated values generally increases as the states become more excited. Achieving a good description of the higher-lying resonances in pyrazine (or in other many electron systems) seems to require the inclusion of higher-lying virtual orbitals as these are needed to sufficiently describe correlation.

A test of convergence of the partial waves expansion was performed by including continuum basis functions with $l = 5$ in the calculation using the cc-pVDZ basis set. We noticed only minor differences in the symmetries B_{3u}, B_{2u}, B_{1u} and A_u with negligible effects on the resonant structures; the effects on the other symmetries (including B_{2g}) could not be tested, because the $l = 5$ continuum functions do not contribute to scattering in these symmetries.

TABLE IV. Positions and widths (in eV) of the π^* resonances in pyrazine calculated in this work at the SEP level and determined by RESON (Ref. 48), a Breit-Wigner profile fitting program. Also listed are the positions of the resonances calculated by Winstead and McKoy (estimated by us from their graphs) and the experimental results of Nenner and Schulz, quoted by listing the centre of the resonance and the range of its vibrational broadening. The range of the $^2B_{2g}$ resonance was estimated by us from the graph of the measured Derivative of the transmitted current.

	$^2B_{3u}$		^2A_u		$^2B_{2g}$	
cc-pVDZ (25 virt.)	0.44	0.032	1.05	0.018	5.38	0.451
cc-pVDZ (35 virt.)	<0		0.79	0.007	4.93	0.453
6-311+G** (40 virt.)	0.14	0.015	1.12	0.030	5.19	0.527
6-311+G** (50 virt.)	<0		0.70	0.006	4.87	0.389
Winstead and McKoy[26]	0.2		1.3		4.4	
Nenner and Schulz[28]	0.065		0.87		4.10	
	0.065–0.8		0.87–1.2		3.8–4.4	

B. Close-coupling calculations

The scattering models for our close-coupling calculations were based on the model B in the work of Dora *et al.*[21] Namely, the L^2 configurations we used take the form:

$$\chi_i^{CC}: \begin{cases} (\text{core})^{N_d}(\text{CAS})^{N-N_d-1}(\text{virtual})^1, \\ (\text{core})^{N_d}(\text{CAS})^{N-N_d+1}, \end{cases} \quad (5)$$

where $N_d = 32$ are electrons frozen in doubly occupied target orbitals and CAS represents the eight orbitals of the active space.

From the excited states listed in the Table I we included in our calculations only those with vertical excitation energies up to 10.03 eV (10.08 eV) for the calculations using the compact (diffuse) basis set and also the $2\,^1B_{1u}$ state, which has been experimentally observed to lie below the 10 eV threshold. For the compact, cc-pVDZ, basis set a total of 27 electronic excited states were included in the close-coupling calculations. In the case of the diffuse basis set, 6-311+G**, a total of 29 electronic excited states were included. Calculations using the compact basis set employed 40 virtual orbitals, while the ones using the diffuse basis set used 70.

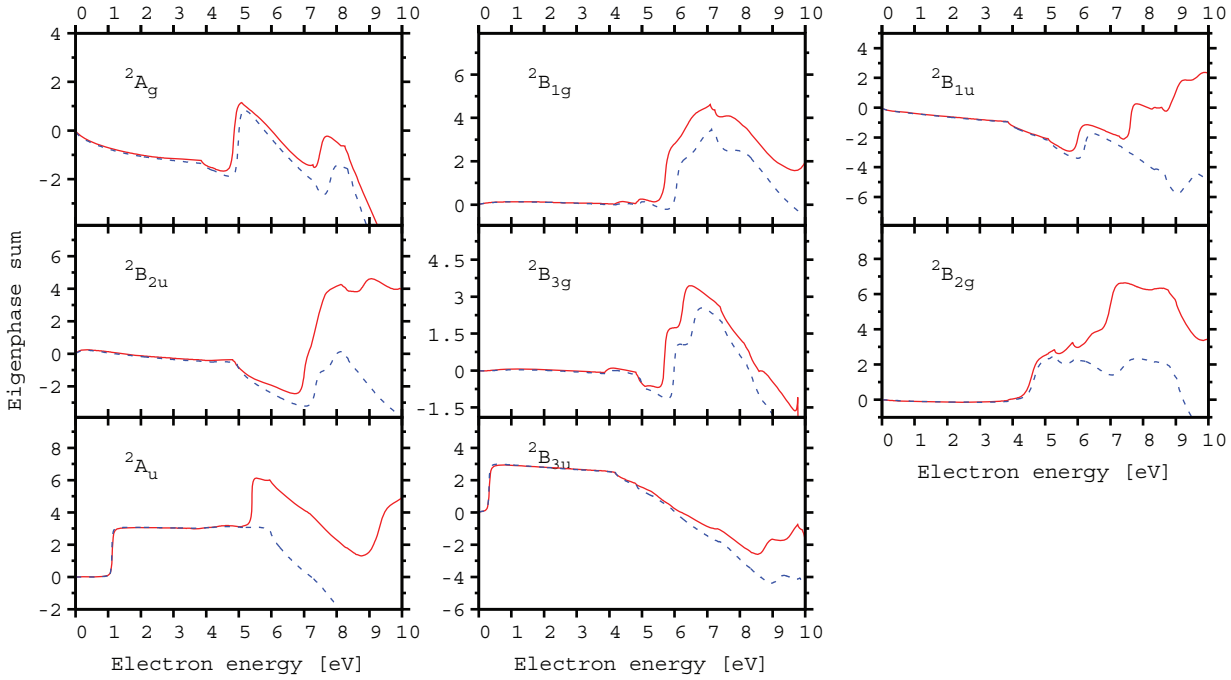

FIG. 4. Eigenphase sums for scattering in all symmetries of pyrazine at the close-coupling level. Solid red: calculations performed using the basis set 6-311+G**, R-matrix radius $a = 18a_0$ and 70 virtual orbitals. Dashed blue: basis set cc-pVDZ, $a = 13a_0$ and 40 virtual orbitals.

In order to achieve a good description of the continuum when the diffuse basis set is used (and $a = 18a_0$ is needed), we are forced to work at the limit of linear dependence. To ascertain whether unphysical R-matrix poles caused by any residual linear dependence between the continuum and the target orbitals are present, we increased the deletion thresholds for the orthogonalization of the continuum functions (up to 4 orders of magnitude for some symmetries). This increase leads to a decrease in the quality of the representation of the continuum that can be observed in the eigenphase sums, but should cause non-physical features due to linear dependence to disappear or at the very least move significantly. The only unstable structure found was the second step in the ^2A_u symmetry, which has been already identified as unphysical in the SE calculations described above.

Figure 4 shows eigenphase sums for our best (with respect to the positions of the three π^* resonances) close-coupling calculations using the compact and the diffuse basis sets. We can see that the eigenphase sums are very structured with many of the features present in the calculations using both basis sets. It is apparent from Figure 4 that use of the diffuse basis set leads to better defined structures in the eigenphase sums and in some symmetries ($^2B_{1u}$ and $^2B_{2u}$) to appearance of additional structures.

The corresponding total cross sections are shown in Figure 5. Summed total integral cross section and inelastic cross sections for scattering into the two lowest-lying electronic excited states are shown in Figure 6 for the diffuse basis set. Elastic differential cross sections for selected energies are shown in Figure 7 for both the SEP and CC models, again using the diffuse basis set. We also tested the use of the scaled continuum basis set as described in Sec. IV A, while retaining the values of the deletion thresholds. The stability of the eigenphase sums was observed again. The results of our close-coupling calculations for symmetries $^2B_{3g}$ and $^2B_{2u}$ shown in Figures 4 and 5 actually used the scaled continuum basis set. It is also worth mentioning that the structures seen in our eigenphase sums moved smoothly towards lower energies as the number of the virtual orbitals included was being increased up to 40 or 70 respectively.

Our scattering codes allow us to individually shift the energies of the target electronic states included in (1). We applied shifts to the vertical excitation energies of those states in Table I for which experimental values are available. We have not observed any significant changes in the positions of the resonant structures present in the calculations. Furthermore, analysis of the L^2 configurations from the results of the calculation using the Simplified model (see below for details) with shifted states gave the same assignment of the resonant structures, with the R-matrix poles describing the resonant structures hardly moving (at most ≈0.19 eV).

1. Assignment of the resonant structures

The three π^* resonances of ^2A_u, $^2B_{3u}$ and $^2B_{2g}$ symmetries are clearly visible in all our calculations. The main aim of this section is to interpret the rest of the structures present in our close-coupling results. We can see from Figure 2 that the eigenphase sums for the SE calculations in symmetries ^2A_g, $^2B_{1g}$, $^2B_{2u}$ and $^2B_{3g}$ are essentially flat in the region below 10 eV, while our close-coupling calculations show numerous resonant-like structures in these symmetries. Somewhat surprisingly these structures are not significantly visible in the corresponding cross sections shown in Figure 5 (with exception of the peaks in $^2B_{1g}$ symmetry). However, most

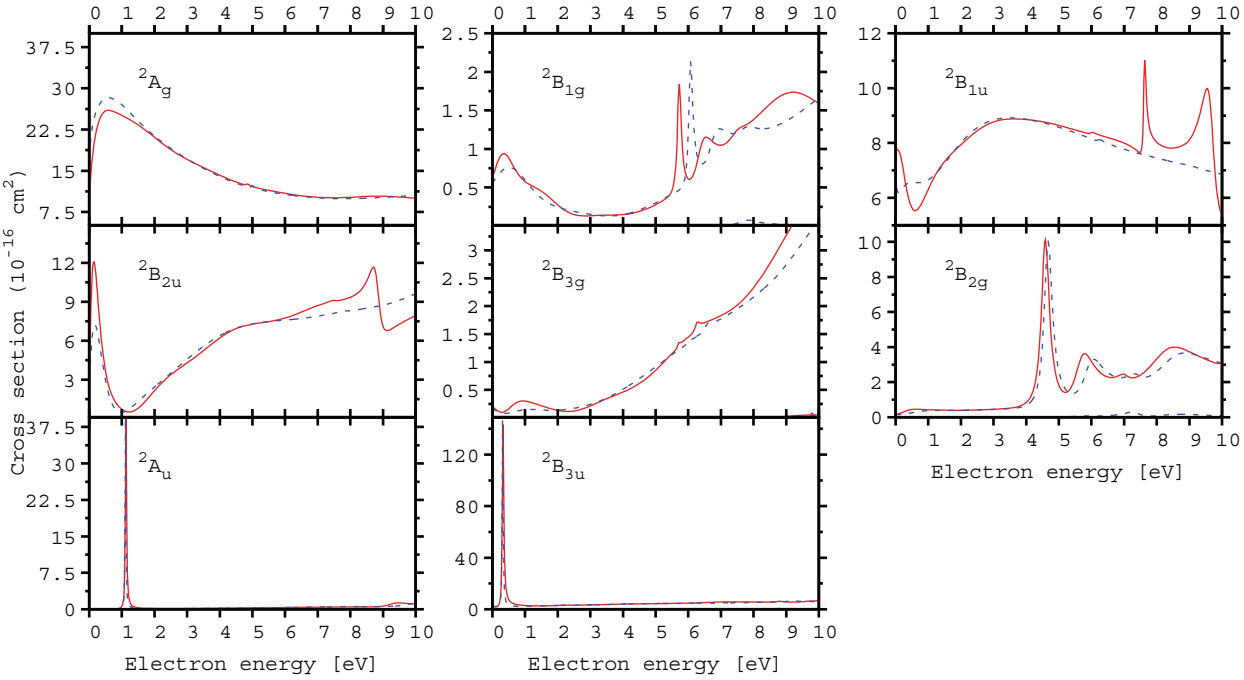

FIG. 5. Contributions to the total cross section from all scattering symmetries at the close-coupling level. Solid red: calculations performed using the basis set 6-311+G**, $a = 18a_0$ and 70 virtual orbitals. Dashed blue: basis set cc-pVDZ, $a = 13a_0$ and 40 virtual orbitals.

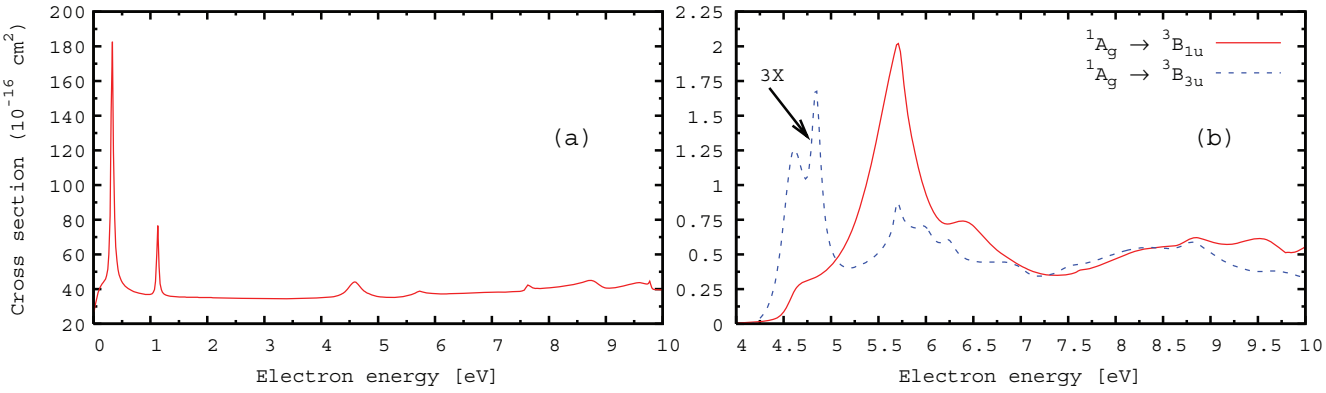

FIG. 6. Cross sections for electron collisions with pyrazine calculated at the close-coupling level using the basis set 6-311+G**, $a = 18a_0$ and 70 virtual orbitals. (a) Integral total (elastic plus inelastic) cross section. (b) Integral cross sections for scattering into the two lowest-lying electronic excited states: $1\,^3B_{1u}$ and $1\,^3B_{3u}$; the cross section for the latter has been multiplied by 3.

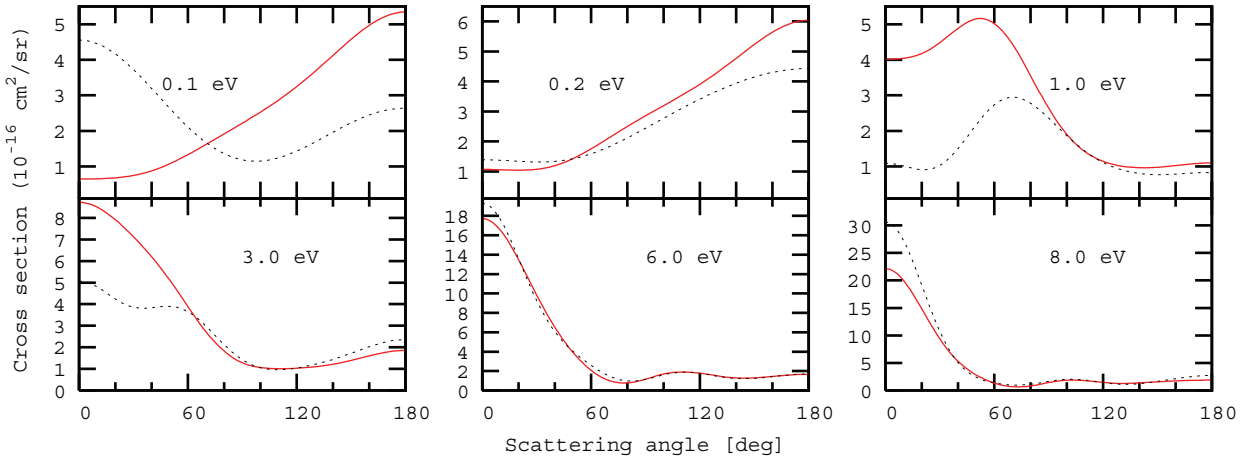

FIG. 7. Differential cross sections calculated using the final SEP (dashed black) and CC (solid red) models in the diffuse basis set for the energies indicated in the panels.

TABLE V. Positions and widths (in eV), along with the main configurations and proposed parent states of the electron resonances in pyrazine from the results of our close-coupling calculations using the 6-311+G** basis set, $a = 18a_0$ and 70 virtual orbitals. If the width of the resonance is given, this and its position were determined using RESON. Otherwise the position was estimated from Figures 4 and 5. Configurations are given in terms of direct products of singly occupied orbitals of the reference HF ground state configuration $(1-6a_g)^{12}1b_{3u}^2(1-4b_{2u})^8 1b_{1g}^2(1-5b_{1u})^{10}1b_{2g}^2 3b_{3g}^6$ and singly or doubly occupied orbitals of the active space. Orbitals in each direct product are grouped from left to right according to their increasing SA-CASSCF energy. Electron spin (up or down) is denoted by α and β and has been replaced by the occupation number 1 in the configurations in which both the singlet and triplet spin symmetries contribute to the given spatial configuration.

Resonance	E_r	Γ_r	Main configuration(s)	Most likely parent state(s)
$1\,^2A_g$	4.85	...	$6a_g^\alpha \otimes 2b_{3u}^2$	$1\,^3B_{3u}$, $2\,^1A_g$
$2\,^2A_g$	7.49	0.22	Not determined	...
$1\,^2B_{3u}$	0.32	0.05	$2b_{3u}^1$	shape character only
$1\,^2B_{2u}$	7.00	0.13	$5b_{1u}^1 \otimes 2b_{3u}^1 \otimes 1a_u^1$	$1\,^3B_{2g}$, $1\,^3B_{1g}$, $1\,^1B_{1g}$
$2\,^2B_{2u}$	7.49	0.25	Not determined	...
$3\,^2B_{2u}$	8.70	...	Not determined	...
$1\,^2B_{1g}$	5.72	0.15	$1b_{2g}^1 \otimes 2b_{3u}^1 \otimes 1a_u^1$ $1b_{1g}^\alpha \otimes 1a_u^2$, $1b_{1g}^\alpha \otimes 2b_{3u}^2$ $1b_{3u}^1 \otimes 1a_u^1 \otimes 2b_{2g}^1$ $1b_{2g}^1 \otimes 2b_{3u}^1 \otimes 1a_u^\alpha$	$1\,^{3?}B_{1u}$, $1\,^?B_{2u}$
$2\,^2B_{1g}$	6.33	0.67	Not determined	...
$1\,^2B_{1u}$	6.03	...	$5b_{1u}^\alpha \otimes 2b_{3u}^2$ $6a_g^1 \otimes 2b_{3u}^1 \otimes 2b_{2g}^1$	$1\,^3B_{2g}$
$2\,^2B_{1u}$	7.61	0.09	Not determined	...
$1\,^2B_{2g}$	4.58	0.30	$2b_{2g}^\alpha$ $1b_{1g}^\alpha \otimes 2b_{3u}^\beta \otimes 1a_u^\alpha$ $1b_{3u}^1 \otimes 1b_{1g}^1 \otimes 2b_{3u}^2 \otimes 1a_u^\alpha$ $1b_{2g}^\beta \otimes 2b_{3u}^2$,$1b_{2g}^\beta \otimes 1a_u^2$	$1\,^3B_{1u}$, $1\,^1B_{2u}$, ground state
$2\,^2B_{2g}$	5.67	...	Not determined	...
$3\,^2B_{2g}$	6.97	0.30	Not determined	...
$1\,^2B_{3g}$	5.69	0.08	$6a_g^1 \otimes 2b_{3u}^1 \otimes 1a_u^1$ $5b_{1u}^1 \otimes 1b_{2g}^1 \otimes 2b_{3u}^2 \otimes 1a_u^1$	$1\,^3A_u$, $1\,^3B_{3u}$
2^2B_{3g}	6.25	0.17	Not determined	...
$1\,^2A_u$	1.13	0.04	$1a_u^1$	shape character only

structures in the eigenphase sum have proven to be very stable, as detailed above. These stable resonances, that we take to be physical, are listed in Table V.

In order to further investigate the resonances and postulate their parent state(s), we performed close-coupling calculations with the first set of L^2 configurations in (5) completely removed from our model, i.e., without the L^2 configurations involving virtual orbitals. Depending on the symmetry the number of L^2 functions generated in this reduced model ranged between 120 and 132 only. We analyzed the most important L^2 configurations contributing to the R-matrix pole closest in energy to an observed resonant structure: we found that the CI coefficients for the main contributing L^2 configurations describing the resonance differed slightly (± 0.15) between the calculations using the diffuse and the compact basis sets, but their relative magnitude was similar, allowing us to classify consistently the configurations according to their importance. We first analyzed the three π^* resonances, whose character is well established[26,28] in order to confirm validity of this approach and then turn to the new structures appearing in our calculations. The assignment of the parent states was done on the basis of correlating the most important L^2 configurations for each resonance with the main configurations responsible for the singlet and triplet excited states of the molecule as determined from the CI vectors for these states resulting from our SA-CASSCF calculations described above. An attempt to perform the same analysis for the full scattering models proved unfeasible, due to the large number of configurations in the CI expansion. A summary of the calculated resonance parameters, their main configurations and their proposed parent states is presented in Table V.

From all the structures observed in our standard calculations, only the first for each spatial symmetry were visible using the Simplified model. The exception is the $^2B_{2g}$ symmetry, where the second structure was visible as well. The first structure in $^2B_{2u}$ symmetry was only visible in the Simplified model calculations using the diffuse basis set. The magnitude of the "step" in the eigenphase sum associated with the observed structures was smaller in the Simplified model and the structures were shifted roughly by 1 eV towards higher energies.

We can now turn to a detailed analysis of the structures listed in Table V.

$1\,^2B_{3u}$ resonance. This π^* resonance can be identified unambiguously as the scattering electron being trapped in the $2b_{3u}$ orbital without exciting the molecule from the ground state (g.s.) HF configuration, hence as a pure shape resonance. The CI coefficient for this configuration has a magnitude of $\approx$0.8.

$1\,^2A_u$ resonance. In this resonance the electron is trapped in the $1a_u$ orbital, while leaving the molecule in its ground state. Therefore, this resonance is also purely shape as expected, without any other L^2 configurations significantly contributing. The CI coefficient for this configuration has the value $\approx$0.6 with the rest of the L^2 configurations having negligible CI coefficients.(The second structure visible in the eigenphase sum is unphysical: it disappears when the deletion thresholds are increased).

$^2B_{2g}$ resonances. We can fully confirm the partial core-excited character of the $1\,^2B_{2g}$ resonance as demonstrated previously by Winstead and McKoy. Unlike the previous two resonances the main, shape-like, configuration (HF g.s.)$^{42} \otimes 2b_{2g}^1$ has now CI coefficient of only $\approx$0.4 with the other configurations listed in the Table V having CI coefficients ranging from $\approx$0.3 to $\approx$0.1. Most of the doublet configurations shown can be thought of as built on the most important singlet and triplet excitations responsible for the $1\,^3B_{1u}$ and $1\,^1B_{2u}$ excited states of pyrazine. Our results do not always allow us to assign unambiguously the triplet or singlet character of the possible parent states: in this case the evidence provided by Winstead and McKoy together with our results favours as the main parent state the $1\,^3B_{1u}$ excited state. This resonance is responsible for the shoulder seen in Figure 6(b) around 4.6 eV in the cross section for excitation of the molecule into the $1\,^3B_{1u}$ excited state. Interestingly, the peaks around 4.6 eV and 5.70 eV in the second inelastic cross section ($^1A_g \rightarrow 1\,^3B_{3u}$) are also caused by significant contributions of this and the $2\,^2B_{2g}$ resonance, but we have not identified as important in the $1\,^2B_{2g}$ resonance the corresponding L^2 configuration built on the main excitation ($6a_g^\alpha \otimes 2b_{3u}^\alpha$) responsible for the $1\,^3B_{3u}$ state. The second $^2B_{2g}$ resonance is barely visible in the Simplified model and we have not attempted to interpret this resonance in terms of configurations. We would like to point out that the third L^2 configuration contributing to the description of the $1\,^2B_{2g}$ resonance as identified by us is based on double excitation of the target molecule, which is a configuration not present in the calculations of Winstead and McKoy. Accounting for this type of configuration in their models could perhaps shift the resonance even closer towards its experimental position.

^2A_g resonances. Figure 4 shows the presence of two structures in this symmetry although the SE results from Figure 2 using the compact basis set do not show any resonances in the whole energy region studied. A detailed examination of the results of the Simplified model then reveals that the most likely parent state responsible for the first core-excited resonance in this symmetry is the $1\,^3B_{3u}$ state. This assignment together with the position of this resonance agree very well with the largest peak in Figure 6 for inelastic scattering into the $1\,^3B_{3u}$ excited state. The $1\,^2A_g$ resonance manifests itself only as a small kink in the corresponding total ^2A_g cross section. The second structure in the eigenphase sum becomes apparent only when a higher number of virtual orbitals is included in the close-coupling model, but it does not show up in the cross section at all, suggesting that this resonance is probably not fully described by our models.

$^2B_{1g}$ resonances. The absence of structures in the SE results suggest that these resonances are of core-excited character, as confirmed by the analysis of the results of our Simplified model. A clear assignment of the spin symmetry of the parent states of the $1\,^2B_{1g}$ resonance based on our results proved to be impossible and we can only say that this resonance contains a significant admixture of singlet and triplet configurations responsible for the lowest-lying excited states of B_{1u} and B_{2u} symmetries. This resonance along with the $2\,^2B_{2g}$ resonance (main contribution) are responsible for the largest peak in the cross section for inelastic scattering $^1A_g \rightarrow 1\,^3B_{1u}$, suggesting that one of the main parent states is probably the $1\,^3B_{1u}$ excited state.

$^2B_{1u}$ resonances. Figure 4 suggests the presence of up to three resonances. The configuration of the second could not be determined. We do not attempt to interpret the third (highest-lying) structure seen in the calculations using the diffuse basis set, because our calculations may become unreliable at these energies. Analysis of the $1\,^2B_{1u}$ resonance in the Simplified model shows the most significant contribution to be from the excitation responsible for the $1\,^3B_{2g}$ excited state. Our SE calculations performed in the diffuse basis set show a significant step around 8 eV and we argue that it corresponds to the second resonance seen in this symmetry in the close-coupling calculations using the diffuse basis set. Close-coupling calculations using the compact basis set show a second structure in the eigenphase sum, which straddles the 10 eV region and probably corresponds to one of the other two structures (above the first one) seen in the calculations using the diffuse basis set.

$^2B_{2u}$ resonances. The lowest resonance of this symmetry can be described in our calculations by only one type of excitation of the target molecule. However, the value of the corresponding CI coefficient is relatively small ($\approx$0.2) and this excitation can correspond to three different parent states: $1\,^3B_{2g}$, $1\,^1B_{1g}$ and $1\,^3B_{1g}$. This resonance is not present in the Simplified model results when the compact basis set is used, suggesting a particular sensitivity to the shape of the target orbitals. We have not been able to identify the origin of the second resonance in this symmetry, but our SE results suggest that it might be associated with one of the higher lying virtual orbitals in this symmetry. The $3\,^2B_{2u}$ resonance might not be physical and the oscillatory behaviour of the eigenphase sum seen above 8 eV may be due to a poor description of the

continuum at higher energies in this symmetry. Nonetheless a third structure was also observed above 10 eV in calculations using the compact basis set, where the description of the continuum is generally much better.

$^2B_{3g}$ resonances. We were able to identify the parent states of the $1\,^2B_{3g}$ resonance as the $1\,^3A_u$ and $1\,^3B_{3u}$ states. Both configurations listed in Table V are built on the two most important target excitations responsible for these excited states. We have not been able to determine the configurations of the second resonance in this symmetry.

V. DISCUSSION

Our analysis shows that the parent states of the first core-excited resonant structures in most of the symmetries are the excited states of the molecule lying below 5 eV. The inelastic cross sections in Figure 6 may provide some hints on the origin of the resonances in Table V that we could not interpret directly by identifying the main L^2 configurations. For example the $2\,^2B_{1g}$ resonance contributes to the shoulder at around 6.3 eV in the cross section for inelastic scattering $^1A_g \rightarrow 1\,^3B_{1u}$ and the series of small peaks in the cross section for the inelastic scattering $^1A_g \rightarrow 1\,^3B_{3u}$ above 5.5 eV are caused by contributions of the $2\,^2B_{2g}$, $1\,^2B_{3g}$ and $2\,^2B_{3g}$ resonances. As suggested in Table V, the resonances do not always have a single parent state, a phenomenon observed in electron collisions even with the simplest molecule H_2.[49]

The resonances present in our calculations above the three π^* ones are not very visible in the total cross sections (see Figure 5); this is not necessarily in disagreement with the experimental findings of Nenner and Schulz, who state:[28] "we did observe another broad structure (in the derivative of the transmitted current) above the third resonance in the diazine spectra, but we do not interpret it." The broad structure to which Nenner and Schulz are referring may correspond to the $1\,^2B_{1g}$ and $2\,^2B_{2g}$ resonances appearing in our calculations around 5.7 eV (see the total integral cross section in Figure 6(a), where these resonances are also visible). The other resonances observed by us (a couple of them are just about visible in the total cross section) are probably too weak to be discerned in the experiment of Nenner and Schulz.

Two resonant structures in our calculations, present at all levels of approximation, posses the appropriate symmetry to correspond to a σ^* shape resonance: the $2\,^2B_{1u}$ feature present at 7.61 eV in the close-coupling calculations and the $2\,^2B_{2u}$ feature present at 7.49 eV. These are significantly narrower than the σ^* resonance characterized by Gianturco *et al.* in their uracil work[19] and our analysis indicated that they probably have some core-excited character; nonetheless one of these might be the pyrazine equivalent of the σ^* uracil resonance. An extremely wide resonance (as postulated by Burrow *et al.*), would probably be undetectable by simple examination and fitting of the eigenphase sums.

Another interesting finding is the remarkable similarity of the positions of the $2\,^2A_g$ and $2\,^2B_{2u}$ resonances and the $2\,^2B_{2g}$ and $1\,^2B_{3g}$ resonances. In the second case we know that the most important configuration (out of the two listed) responsible for the $1\,^2B_{3g}$ resonance is the $6a_g^1 \otimes 2b_{3u}^1 \otimes 1a_u^1$. We can see that replacing the highest-energy orbital $1a_u$ in this configuration (and also in the second one) by the $6b_{1u}$ orbital, which even lies close in energy to the $1a_u$ orbital (see Table II), yields a configuration of $^2B_{2g}$ symmetry, suggesting that some of the resonances (e.g., $2\,^2B_{2g}$ and $1\,^2B_{3g}$) may correspond to the same parent state, with the scattering electron trapped in a different orbital. As mentioned above, the resonance $2\,^2B_{2g}$ is barely visible in the simplified close-coupling model, which does not include the orbital $6b_{1u}$, suggesting that this resonance is probably not sufficiently well described by the L^2 configurations at this level. We can further support the hypothesis outlined above by comparing the main configurations responsible for the $1\,^2B_{3g}$ and $1\,^2A_g$ resonances, which differ only by the placement of the scattering electron in the $1a_u$ orbital and in the $2b_{3u}$ orbital respectively. The positions of these resonances are then consistent with the fact that the $2b_{3u}$ orbital is energetically lower than $1a_u$. The same type of behaviour also occurs for the $1\,^2B_{2u}$ and $1\,^2B_{1u}$ resonances.

We have seen that our close-coupling calculations based on the Simplified model display half of the resonant structures seen in our final results. We ascribe this to the active space (10, 8) being too small to describe these structures well: for example the $1\,^2B_{2u}$ resonance is not present in the Simplified model results when the compact basis set is used, but becomes clearly visible when a high number of virtual orbitals is used in the scattering model. The virtual orbitals are clearly essential to properly describe these resonances.

Going back to the results of our SEP calculations, we see that the position of the third π^* resonance as calculated by Winstead and McKoy is in better agreement with the experimental data than our results. The SEP models of Winstead and McKoy make use of the MVOs rather than HF or CASSCF orbitals. It would seem that it is the choice of the scattering model of Winstead and McKoy (which uses *all* virtual orbitals) together with the use of MVOs, which is responsible for the better results for the position of the third shape resonance. We attribute this to their scattering model providing a more balanced description of electron correlation at all energies of interest ($\approx$0−10 eV). In our SEP models, bringing the third π^* resonance closer to its experimental position (by inclusion of more virtual orbitals) causes the overcorrelation of the other two π^* resonances, which then appear too low in energy. It should be noted that even in our highest-level close-coupling calculations accurate modeling of the short range correlation has proved extremely difficult.

The use of atomic orbital basis set with diffuse functions on all atoms in the calculations of Winstead and McKoy seems to be essential for obtaining a good set of MVOs. A similar effect is observed in our calculations: we can see from the Table I that the use of the diffuse basis set does not improve the description of the target excited states, however, its use is important for description of the scattering electron, particularly at lower energies as we can see from the calculated cross sections.

Figure 7 shows that the CC and SEP models give different results for the differential cross sections at very low energies (<1 eV). We explain this difference by the absence of the Ramsauer-Townsend minimum in the ^2A_g symmetry in the

CC calculations, the most significant difference in the integral cross sections at low energies. The differential cross sections for 6 and 8 eV agree fairly well with those of Winstead and McKoy; at 1 and 3 eV it's our SEP cross section that agrees better whereas in the very low energy range (where in fact, nuclear motion effects should not be neglected as we do) the cross sections are fairly different.

The three Feshbach resonances of $^2A'$ symmetry (at 6.17 eV, 7.62 eV and 8.12 eV) found by Dora *et al*. in uracil may correspond to resonances in ^2A_g, $^2B_{3g}$, $^2B_{1u}$ and $^2B_{2u}$ symmetries found by us in pyrazine, but an assignment based on the energies of these resonances is not unambiguous, and therefore we do not correlate the core-excited resonances found in pyrazine with the Feshbach resonances found in uracil. Additionally, our analysis indicates that most if not all the resonances we observe in pyrazine do not have a clear Feshbach character, as they appear at energies above at least one of their likely parent states.

It is apparent from Table V that many of the core-excited resonances in pyrazine are built on the excitations from the lone-pair σ orbitals $6a_g$ and $5b_{1u}$ located on the two nitrogen atoms. Whether the inclusion of more sigma orbitals in the active space for the uracil calculations may lead to the appearance of similar resonances will depend on the character of these orbitals.

Our last remark, regarding scattering models for pyrazine in general concerns the fact that this molecule possesses at least one bound negative ion state of $^2B_{3u}$ symmetry. Accordingly, Nenner and Schulz interpreted the $1\,^2B_{3u}$ and $1\,^2A_u$ resonances in terms of excited (and ground) vibrational levels of the ground (and the first excited) electronic state of the negative ion. An example of an SEP calculation in which the $1\,^2B_{3u}$ resonance becomes bound was shown in Sec. IV A 1. We can not ascertain which scattering result (the anion $^2B_{3u}$ state being bound or resonant) is more physical in our fixed nuclei calculations. However, our trial CASSCF calculations on the negative ion (at the ground state equilibrium geometry of the neutral), place the lowest-lying state of $^2B_{3u}$ symmetry above the energy of the neutral ground state, hence we chose to present as more internally consistent the results of models which retain the $^2B_{3u}$ state as a resonance.

VI. CONCLUSIONS

We present the first calculations to fully incorporate inelastic channels in the study of electron collisions with pyrazine. Our results confirm the experimental and prior theoretical findings related to the three lowest π^* resonances, both in terms of their positions and their character. Our calculations also show the presence of a larger than expected number of core-excited resonances. This result is however, compatible with experimental evidence[13] for the presence of many resonances (more accurately, peaks in the yield of various anions) in the 5–10 eV range in uracil. These resonances do not necessarily have a single parent state. A number of tests were performed, most of them geared towards identifying and eliminating non-physical features from our results. The resonances listed in Table V proved stable and persisted in the various tests detailed above.

We have shown the need to look at the appropriateness of the basis sets to represent not only the occupied target orbitals, but also those virtual orbitals required to provide a good representation of the correlation-polarization. The eigenphase sums from the close-coupling calculation show that the higher-lying resonant structures are more clearly visible when a diffuse basis set is used. It should be noted that inclusion of more virtual orbitals in our calculation with the compact basis set improves the representation of the higher-lying resonances but overcorrelates the lower energy ones significantly. We can say that the diffuse basis set provides a more 'balanced' description of the correlation-polarization effects. We therefore conclude that in the models of our type, one should choose a basis set that provides a good description of the properties (transition moments, energies, etc.) of the relevant target electronic states, but *also* of the short range electron correlation in the *scattering* calculations.

The close-coupling model labelled B by Dora *et al*.[21] is transferable to other pyrimidine-like molecules. These systems are likely to posses, like pyrazine, a number of higher-lying core-excited resonances built mainly upon the triplet electronic excited states of the molecule that could be studied with our techniques. Dora *et al*. found 15 virtual orbitals per symmetry optimal, which makes it a total of 30 lowest-lying orbitals used in their calculations on uracil. In our calculations on pyrazine 40 lowest-lying orbitals were found to be the optimal number. Pyrazine has 42 electrons whereas uracil 58. We therefore conclude that the close-coupling models using about 30–40 virtual orbitals and a compact basis set are easily transferable to scattering calculations on different pyrimidine-like targets. We expect a similar transferability to be applicable to calculations using the diffuse basis set.

These models, however, are probably not final and more work is needed towards formulating more sophisticated ones, once the computational implementations are in place (work is already under way to ensure much larger Hamiltonians can be diagonalized in the R-matrix suite; this would allow us to use larger active spaces as well as consider the introduction of pseudostates in the close-coupling expansion in order to better describe the polarization of the target[50,51]). In addition, due to the need to use diffuse basis sets, the ability to perform calculations for bigger R-matrix radii is also required; this will entail a re-think of the basis functions used to describe the scattering electron. These more sophisticated models will hopefully provide a better description (and more accurate parameters) of all the resonant structures observed in our calculations.

Experimental cross sections for pyrazine, in particular differential cross sections, would greatly contribute to helping us choose the best models: the Ramsauer-Townsend minimum observed in SEP models but absent from the CC calculation is not visible in the integral cross section.

ACKNOWLEDGMENTS

This work was supported by the EPSRC. We thank Professor Vincent McKoy for useful discussions on the resonant structures in pyrazine.

[1]B. Boudaïffa, P. Cloutier, D. Hunting, M. A. Huels, and L. Sanche, Science, **287**, 1658 (2000).
[2]L. Sanche, Eur. Phys. J. D **35**, 367 (2005).
[3]R. Barrios, P. Skurski, and J. Simons, J. Phys. Chem. B **106**, 7991 (2002).
[4]J. Simons, Acc. Chem. Res **39**, 772 (2006).
[5]K. Aflatooni, G. Gallup, and P. Burrow, J. Phys. Chem. A **102**, 6205 (1998).
[6]A. Scheer, K. Aflatooni, G. Gallup, and P. Burrow, Phys. Rev. Lett. **92**, 068102 (2004).
[7]G. A. Gallup and I. I. Fabrikant, Phys. Rev. A **83**, 012706 (2011).
[8]A. M. Scheer, C. Silvernail, J. A. Belot, K. Aflatooni, G. A. Gallup, and P. D. Burrow, Chem. Phys. Lett. **411**, 46 (2005).
[9]F. Martin, P. D. Burrow, Z. Cai, P. Cloutier, D. Hunting, and L. Sanche, Phys. Rev. Lett. **93**, 068101 (2004).
[10]S. Ptasińska, S. Denifl, B. Mróz, M. Probst, V. Grill, E. Illenberger, P. Scheier, and T. D. Märk, J. Chem. Phys. **123**, 124302 (2005).
[11]P. D. Burrow, G. A. Gallup, A. M. Scheer, S. Denifl, S. Ptasinska, T. Märk, and P. Scheier, J. Chem. Phys. **124**, 124310 (2006).
[12]H. Hotop, M. Rul, and I. I. Fabrikant, Phys. Scr. **110**, 22 (2004).
[13]S. Denifl, S. Ptasińska, G. Hanel, B. Gstir, M. Probst, P. Scheier, and T. D. Märk, J. Chem. Phys. **120**, 6557 (2004).
[14]S. Denifl, S. Ptasińska, M. Probst, J. Hrušák, P. Scheier, and T. D. Märk, J. Phys. Chem. A **108**, 6562 (2004).
[15]K. Aflatooni, A. M. Scheer, and P. D. Burrow, J. Chem. Phys. **125**, 054301 (2006).
[16]S. Ptasińska, S. Denifl, V. Grill, T. D. Märk, E. Illenberger, and P. Scheier, Phys. Rev. Lett. **95**, 093201 (2005).
[17]M. Bazin, M. Michaud, and L. Sanche, J. Chem. Phys. **133**, 155104 (2010).
[18]F. A. Gianturco and R. R. Lucchese, J. Chem. Phys. **120**, 7446 (2004).
[19]F. A. Gianturco, F. Sebastianelli, R. R. Lucchese, I. Baccarelli, and N. Sanna, J. Chem. Phys. **128**, 174302 (2008).
[20]C. Winstead and V. McKoy, J. Chem. Phys. **125**, 174304 (2006).
[21]A. Dora, J. Tennyson, L. Bryjko, and Tanja van Mourik, J. Chem. Phys. **130**, 164307 (2009).
[22]C. Winstead, V. Mckoy, and S. Sanchez, J. Chem. Phys. **127**, 085105 (2007).
[23]S. Tonzani and C. H. Greene, J. Chem. Phys. **124**, 054312 (2006).
[24]A. Grandi, F. A. Gianturco, and N. Sanna, Phys. Rev. Lett. **93**, 048103 (2004).
[25]S. Yalunin and S. B. Leble, Eur. Phys. J. Spec. Top. **144**, 115–122 (2007).
[26]C. Winstead and V. McKoy, Phys. Rev. A **76**, 012712 (2007).
[27]C. Winstead and V. McKoy, Phys. Rev. Lett. **98**, 113201 (2007).
[28]I. Nenner and G. J. Schulz, J. Chem. Phys. **62**, 1747 (1975).
[29]I. C. Walker and M. H. Palmer, Chem. Phys. **153**, 169 (1991).
[30]K. K. Innes, I. G. Ross and W. R. Moomaw, J. Mol. Spectrosc. **132**, 492 (1988).
[31]M. Oku, Y. Hou, X. Xing, B. Reed, H. Xu, Ch. Chang, Ch.-Y. Ng, K. Nishizawa, K. Ohshimo, and T. Suzuki, J. Phys. Chem. A **112**, 2293 (2008).
[32]C. Woywod, A. Papp, G. Halsz, and A. Vibk, Theor. Chim. Acta **125**, 521 (2010).
[33]Y. Li, J. Wan, and X. Xu, J. Comput. Chem. **28**, 1658 (2007).
[34]P. Weber and J. Reimers, J. Phys. Chem. A **103**, 9821 (1999).
[35]M. Fulscher and B. Roos, Theor. Chim. Acta **87**, 403 (1994).
[36]M. P. Fulscher, K. Andersson, and B. O. Roos, J. Phys. Chem. **96**, 9204 (1992).
[37]R. J. Suffolk, J. Electron Spectrosc. Relat. Phenom. **3**, 53 (1974).
[38]ukrmol-in, version 0.1, 2010, http://ccpforge.cse.rl.ac.uk/gf/project/ukrmol-in/, ukrmol-out, 2010, http://ccpforge.cse.rl.ac.uk/gf/project/ukrmol-out/.
[39]J. Tennyson, Phys. Rep. **491**, 29 (2010).
[40]P. G. Burke and K. A. Berrington, *Atomic and Molecular Processes: An R-matrix approach* (IOP, Bristol, 1993).
[41]J. Tennyson, J. Phys. B: At. Mol. Phys. **29**, 6185 (1996).
[42]C. W. Bauschlicher, J. Chem. Phys. **72**, 880 (1980).
[43]H.-J. Werner, P. J. Knowles, R. Lindh, F. R. Manby, M. Schütz, *et al*., 2009, MOLPRO, version 2009.1, a package of *ab initio* programs.
[44]A. Faure, J. D. Gorfinkiel, L. A. Morgan, and J. Tennyson, Comput. Phys. Commun. **144**, 224 (2002).
[45]D. Bouchiha, J. D. Gorfinkiel, L. G. Caron, and L. Sanche, J. Phys. B: At., Mol. Opt. Phys. **39**, 975 (2006).
[46]M. Tarana and J. Tennyson, J. Phys. B: At., Mol. Opt. Phys. **41**, 205204 (2008).
[47]M. Tarana, B. M. Nestmann, and J. Horáček, Phys. Rev. A **79**, 012716 (2009).
[48]J. Tennyson and C. J. Noble, Comput. Phys. Commun. **33**, 421 (1984).
[49]D. T. Stibbe and J. Tennyson, J. Phys. B: At., Mol. Opt. Phys. **30**, L301 (1997).
[50]J. D. Gorfinkiel and J. Tennyson, J. Phys. B: At., Mol. Opt. Phys. **37**, L343 (2004).
[51]J. D. Gorfinkiel and J. Tennyson, J. Phys. B: At., Mol. Opt. Phys. **38**, 1607 (2005).